
This is an electronic reprint of the original article.
This reprint may differ from the original in pagination and typographic detail.

Davodi, Fatemeh; Tavakkoli, Mohammad; Lahtinen, Jouko; Kallio, Tanja

Straightforward synthesis of nitrogen-doped carbon nanotubes as highly active bifunctional electrocatalysts for full water splitting

Published in:
Journal of Catalysis

DOI:
[10.1016/j.jcat.2017.07.001](https://doi.org/10.1016/j.jcat.2017.07.001)

Published: 01/09/2017

Document Version
Publisher's PDF, also known as Version of record

Published under the following license:
CC BY-NC-ND

Please cite the original version:
Davodi, F., Tavakkoli, M., Lahtinen, J., & Kallio, T. (2017). Straightforward synthesis of nitrogen-doped carbon nanotubes as highly active bifunctional electrocatalysts for full water splitting. *Journal of Catalysis*, 353, 19-27. <https://doi.org/10.1016/j.jcat.2017.07.001>

This material is protected by copyright and other intellectual property rights, and duplication or sale of all or part of any of the repository collections is not permitted, except that material may be duplicated by you for your research use or educational purposes in electronic or print form. You must obtain permission for any other use. Electronic or print copies may not be offered, whether for sale or otherwise to anyone who is not an authorised user.



Straightforward synthesis of nitrogen-doped carbon nanotubes as highly active bifunctional electrocatalysts for full water splitting



Fatemeh Davodi^a, Mohammad Tavakkoli^a, Jouko Lahtinen^b, Tanja Kallio^{a,*}

^a Department of Chemistry and Materials Science, School of Chemical Engineering, Aalto University, P.O. Box 16100, FI-00076 Aalto, Finland

^b Department of Applied Physics, School of Science, Aalto University, P.O. Box 15100, FI 00076 Aalto, Finland

ARTICLE INFO

Article history:

Received 21 March 2017

Revised 31 May 2017

Accepted 2 July 2017

Available online 22 July 2017

Keywords:

Nitrogen doped carbon nanotube

Oxygen evolution reaction

Hydrogen evolution reaction

Electrolysis

Metal-free catalyst

ABSTRACT

The success of intermittent renewable energy systems relies on the development of energy storage technologies. Particularly, active and stable water splitting electrocatalysts operating in the same electrolyte are required to enhance the overall efficiency and reduce the costs. Here we report a precise and facile synthesis method to control nitrogen active sites for producing nitrogen doped multi-walled carbon nanotube (NMWNT) with high activity toward both oxygen and hydrogen evolution reactions (OER and HER). The NMWNT shows an extraordinary OER activity, superior to the most active non-metal based OER electrocatalysts. For OER, the NMWNT requires overpotentials of only 320 and 360 mV to deliver current densities of 10 and 50 mA cm⁻² in 1.0 M NaOH, respectively. This metal-free electrocatalyst also exhibits a proper performance toward HER with a moderate overpotential of 340 mV to achieve a current density of 10 mA cm⁻² in 0.1 M NaOH. This catalyst also shows high stability after long-time water oxidation without notable changes in the structure of the material. It is revealed that the electron-withdrawing pyridinic N moieties in the NMWNTs could serve as the active sites for OER and HER. Our findings open up new avenues for the development of metal-free electrocatalysts for full water splitting.

© 2017 The Authors. Published by Elsevier Inc. This is an open access article under the CC BY-NC-ND license (<http://creativecommons.org/licenses/by-nc-nd/4.0/>).

1. Introduction

Fossil fuels are currently the dominating energy source and form the basis of the world economy. However, in the future energy supply based on clean and renewable energy will dominate over the dependency on fossil fuels and this addresses challenges for technology development [1,2]. Water electrolysis is a promising method for storing intermittent electrical energy from renewable resources, such as sun and wind, in the form of hydrogen fuel [3]. Electrochemical water splitting in alkaline media includes two half reactions: the hydrogen evolution reaction (HER, $4\text{H}_2\text{O} + 4\text{e}^- \rightarrow 4\text{OH}^- + 2\text{H}_2$) and the oxygen evolution reaction (OER, $4\text{OH}^- \rightarrow 2\text{H}_2\text{O} + 4\text{e}^- + \text{O}_2$). Currently, Ir or Ru-based compounds have shown high activity toward OER in acidic and alkaline media [4,5], and among the non-noble metal OER electrocatalysts, nickel (Ni) based electrocatalysts have shown very promising performance for OER in alkaline media [6–10]. For HER, Pt based materials are known as the most efficient HER catalysts in both acidic and alkaline media [4,11]. However, platinum group metals suffer from high costs and scarcity resulting in difficulties in the long-term availability. Hence, to ensure availability of catalysts innovative

breakthroughs are needed in order to develop affordable, sustainable and efficient catalytic materials for both HER and OER. In order to reduce/replace noble metal based electrocatalysts, various non-precious metal water-splitting catalysts have been developed [12].

In recent years, clear progress has been made in the development of efficient electrocatalysts with earth-abundant materials for HER [13,14] and OER [3,4,15] in alkaline media. Substantial research efforts have been put on developing versatile bifunctional catalysts with satisfying activity toward both HER and OER, enabling operation in the same electrolyte [8,16]. However, developing such active bifunctional electrocatalysts is challenging due to the incompatibility of pH ranges in which catalysts are stable and active. In this view, various efficient bifunctional catalysts based on transition-metal based compounds of Ni [6,8,17–20], Co [4,16,21] and doped heteroatoms [22–24] in alkaline media have been proposed. However, the transition metal oxide materials suffer from intrinsically low conductivity limiting their performance at high current densities. To circumvent this issue, conductive materials such as carbon nanomaterials, graphene and carbon nanotubes (CNTs) are usually used as catalyst supports for transition metal oxide nanoparticles [25,26]. Such carbon supports are inactive toward most of the electrochemical reactions. However, the graphite or carbonaceous materials can be doped by heteroatoms

* Corresponding author.

E-mail address: tanja.kallio@aalto.fi (T. Kallio).

such as nitrogen [24,27], boron [28] or phosphorous [22] to form active metal-free electrocatalysts. Carbonaceous doped materials can be used either as metal-free electrocatalysts [29,30] or as catalyst supports [31] for active metal nanoparticles to get the advantage of synergistic catalytic activity. The chemical and electronic properties of these doped materials can significantly alter their OER and HER performance because of the induced changes in the local charge density and asymmetry spin density of the carbon lattice [32]. Among the carbonaceous doped-materials, nitrogen doped CNTs (NCNTs) have recently gained notable attention as low-cost metal-free catalysts with excellent durability, unique structure and earth-abundant element based catalytic active sites [24,27,33–36]. Bin Yang et al. [37] have shown that pyridinic nitrogens serve as the active sites for OER. However, the vast challenge in the NCNTs electrocatalysts is to find a synthesis process enabling control of the final nitrogen types as well as the interaction of nitrogen moieties with the CNTs. Despite tremendous efforts, great challenges exist for developing metal-free electrocatalysts for full water splitting exhibiting the above mentioned features. Hence, only few successful materials have been achieved so far [38].

In this study, nitrogen doped multi-walled carbon nanotubes (NMWNT) are synthesized by a simple, cost-effective and scalable method. These NMWNTs exhibit superior electrocatalytic activity as bifunctional metal-free catalysts toward both OER and HER with excellent stability. Interestingly, the NMWNTs not only show much higher catalytic performance compared to corresponding single-heteroatom-doped counterparts but also show comparable, or even higher, activity than the most active metal-based electrocatalysts, especially the ones reported for OER so far.

2. Results and discussion

The NMWNTs were synthesized as depicted in Fig. 1. The synthesis method is explained in detail in the [Supplementary Information. Scheme S1](#) shows the chemical structure of the emeraldine salt. Shortly, to enhance interaction of MWNTs with emeraldine salt (ES), both commercial MWNTs and ES are first dispersed in

0.0025 M HCl solution (pH 2.6) to create a stable solution [39]. The mixture is then sonicated for 20 h via an ultrasonic bath to provide a very thin and highly interconnected layer of the ES on the surfaces of the MWNT. During this step, the positively charged nitrogen moieties in the polymer induce intimate interaction between ES and MWNT and facilitate the formation of a hybrid material [40]. Thus, the polymer is wrapped simply around the surfaces of the nanotubes through physical adsorption requiring no additional functional group or pretreatment for the nanotubes (see Fig. 2a). Subsequent centrifugation process eliminated the excess polymer and led to separation of the MWNT/ES materials with a low amount of nitrogen of (0.5 at.%). For the comparison two samples with shorter sonication times of 5 and 10 h were prepared leading to nitrogen contents of 1.2 at.% and 1 at.%, respectively, and also one sample with longer sonication time of 30 h were prepared (see [Experimental section in Supporting Information](#)).

The MWNT/ES materials were then pyrolyzed at 800 °C in argon, leading to the formation of surface doped NMWNTs. The final products were denoted as 5, 10, 20 and 30-NMWNT referring to the NMWNTs prepared with different sonication times of 5, 10, 20 and 30 h, respectively.

To investigate the properties of the NMWNT material high-resolution transmission electron microscopy (HRTEM) is utilized to observe the polymer wrapping around the MWNT surface in 20-MWNT/ES before pyrolysis (Fig. 2a) and the changes in the graphitic structure of the 20-NMWNT after pyrolysis (Fig. 2b). Fig. 2a illustrates the presence of thin layer of the residual polymer on the surface of the MWNTs that plays a crucial role in obtaining the material with a high electrocatalytic activity. Moreover, as shown in Fig. 2b the graphite structure of the MWNTs still exhibits a relatively high degree of crystallinity indicating that the sonication and pyrolysis processes do not significantly affect the quality of the nanotubes (see also Fig. S1). This is in agreement with the graphite structure of the 20-NMWNT shown in Raman results (see discussion below).

2.1. OER electrocatalytic activity

The electrocatalytic activity of the 20-NMWNT samples for the OER is investigated by rotating disk electrode (RDE) and rotating ring-disk electrode (RRDE) measurements using a standard three and four-electrode systems, respectively, in 0.1 and 1 M NaOH. Fig. 3a exhibits polarization curves for OER on the 20-NMWNT material compared with the pristine MWNT, IrO₂, and 20 wt% Pt/C electrodes in 0.1 M NaOH saturated with O₂. All the studied catalysts are measured on a glassy carbon (GC) electrode and with a similar loading of ~0.2 mg cm⁻². The 20-NMWNT sample shows a superior OER catalytic activity with an onset potential of 1.54 V versus reversible hydrogen electrode (RHE) in 0.1 M NaOH. The pristine MWNT shows almost no catalytic activity for OER indicating that the activity is induced by the functionalization.

The observed current on the studied electrodes can result from the desired four electron transfer OER (OER pathway: 4OH⁻ → O₂ + 2H₂O + 4e⁻) or from the undesirable two electron transfer reaction (3OH⁻ → HO₂⁻ + 2e⁻ + H₂O) resulting in peroxide formation. Moreover, oxidation of the catalyst material can take place as an unwanted side reaction. To investigate the origin of the high current on 20-NMWNT, RRDE measurements in N₂-saturated 0.1 M NaOH are performed as shown in Fig. 3b. In the RRDE measurements, the oxygen evolved at the catalyst covered glassy carbon disk is subsequently reduced at the surrounding Pt ring electrode hold at 0.4 V. Meanwhile, the ring current resulting from oxygen reduction reaction (ORR) is recorded. Similarly, the Pt ring is held at 1.4 V to reduce any formed H₂O₂ [41,33,42]. In alkaline solution any formed CO₂ (from the catalyst material oxidation) would react

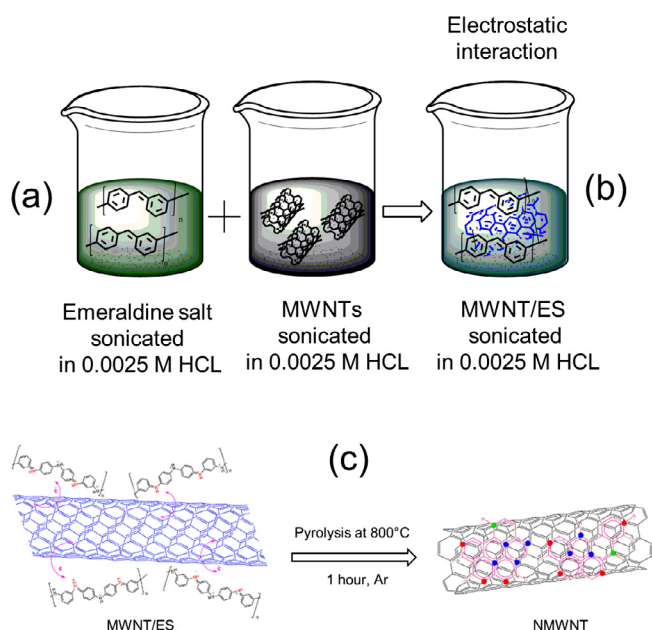


Fig. 1. Schematic illustration of the synthesis procedure of the NMWNT materials. Steps: (a) dispersing emeraldine salt and MWNTs in 0.0025 M HCl; (b) preparing MWNT/ES with electrostatic interaction; and (c) pyrolyzing MWNT/ES to form NMWNT.

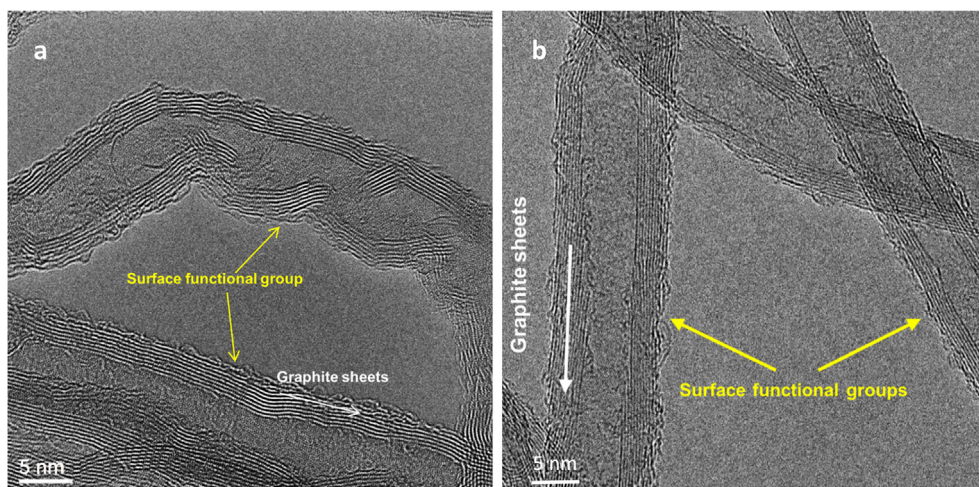


Fig. 2. HRTEM images of (a) before pyrolysis (20-MWNT/ES) and, (b) after pyrolysis 20-NMWNT.

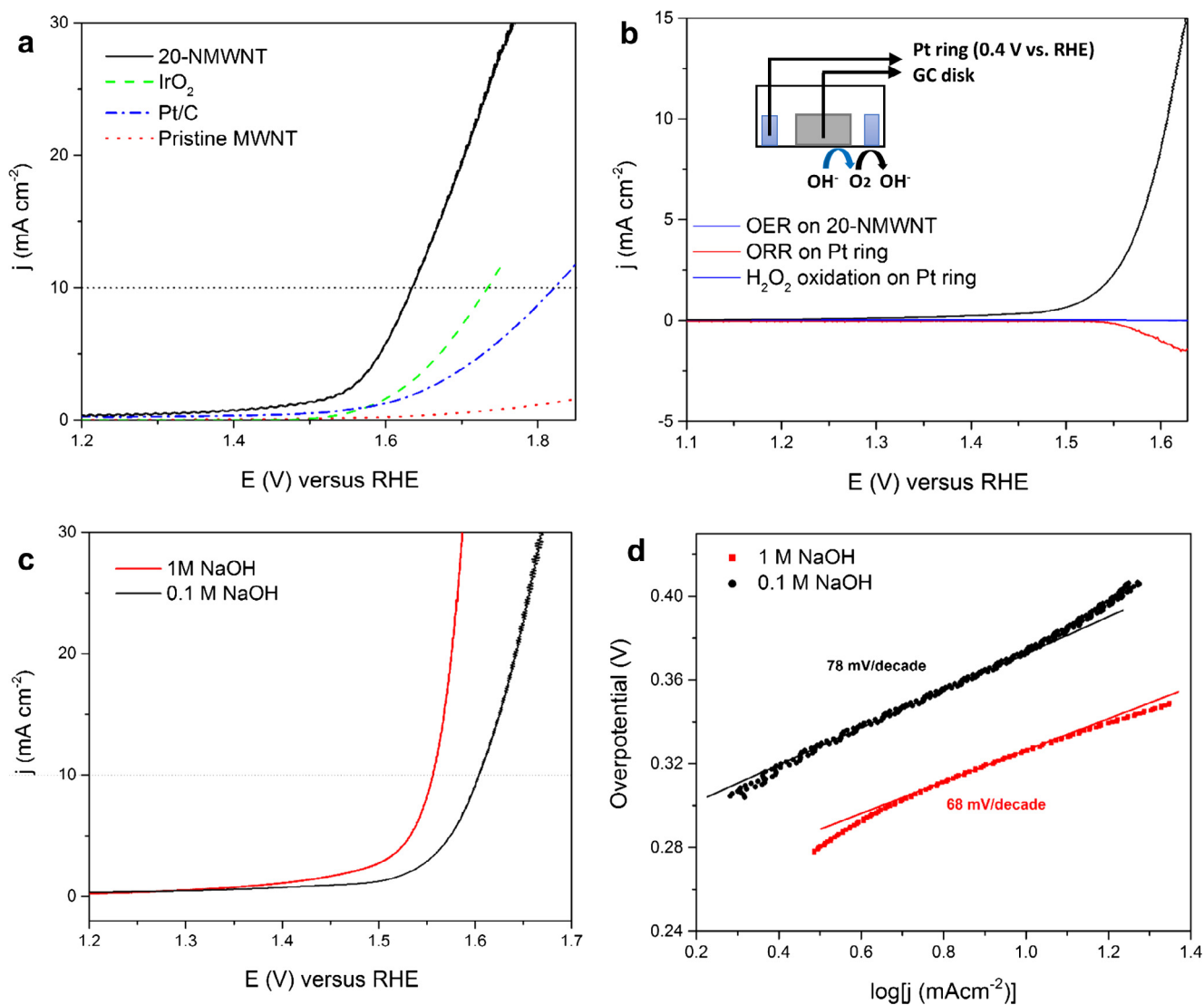


Fig. 3. (a) The RDE polarization curves obtained with 20-NMWNT, IrO₂, Pt/C (20 wt%), and pristine MWNT in 0.1 M NaOH solution. (b) Detection of O₂ evolution from the 20-NMWNT catalyst in 0.1 M NaOH solution using the RRDE measurements (inset shows the schematic of RRDE detection for ORR on the Pt ring caused by OER on the disk). The oxygen evolved during the anodic potential sweep on the disk is subsequently reduced at the Pt ring held at a constant potential of 0.4 V. (c) OER polarization curves NMWNT with iR compensation attained in 0.1 and 1 M NaOH and (d) corresponding Tafel slopes obtained with the 20-NMWNT electrode in 0.1 NaOH and 1 M NaOH. The polarization curves were measured at a scan rate of 5 mV s⁻¹ and a rotation of 1600 rpm.

to carbonate anion which cannot induce any ring current at the used potentials.

As Fig. 3b shows only ORR current at the Pt ring electrode is detected while the disk potential is above the onset of OER (1.53 V). Furthermore, no detectable current from H_2O_2 oxidation at the Pt ring is measured, showing that H_2O_2 is not produced, or its production is under the detection limit, on 20-NMWNT covered disk electrode during OER. The RRDE measurements is also used for calculating the approximate Faradaic efficiency of O_2 evolution (ε), through the equation of $j_{\text{ORR}}/j_{\text{OER}} \times N$, where j_{ORR} and j_{OER} are current densities measured on the Pt ring and the glassy carbon disk, respectively, and N is the collection efficiency of the RRDE [37,43]. For parallel RRDE measurements, $\varepsilon > 90\%$ is calculated for the OER on the 20-NMWNT electrode. Moreover, a similar $\varepsilon > 90\%$ is measured for the same catalyst material in 1 M NaOH electrolyte (Fig. S2).

Since the OER polarization curve of MWNTs, in comparison to NMWNTs, shows almost no anodic current, thus the contribution of oxidation current of carbonaceous materials from the pristine MWNTs in the OER current is also considered almost negligible. Therefore, the current in OER polarization curves originates almost only from the formation of oxygen. The reason that the $\varepsilon > 90\%$ is reported is based on the fact that in RRDE method, it should be noted that small errors in the ring current and collection efficiency can lead to relatively large errors in ε , and thus RRDE measurements are useful for fast screening the approximate faradaic efficiency [10]. Number of other parameters also affect the measured faradaic efficiency by RRDE, such as the bubble formation on the disk hindering O_2 dissolution in the electrolyte and the error in the measured geometric surface area of the disk resulting from inhomogeneous catalyst dispersion. Fig. S3 shows the formation of oxygen bubbles on the 20-NMWNT loaded carbon cloth electrode at a potential of 1.65 V vs. RHE in 0.1 M NaOH. Hence, these results revealed that water oxidation via the 4-electron transfer pathway for generating O_2 is the dominant process on the 20-NMWNT catalyst.

Fig. 3c shows OER polarization curves with iR compensation attained for the 20-NMWNT material in 0.1 and 1 M NaOH. The OER activity of 20-NMWNT is significantly improved in 1 M NaOH and shows an onset potential of only ~ 1.5 V. The overpotentials required for OER current density of 10 mA cm^{-2} (denoted as $\eta_{\text{OER}10}$) are measured to be 360 mV and 320 mV in 0.1 and 1 M NaOH, respectively. These values are comparable to those of the recently reported highly active transition metals [17,25,26,44–46] and superior to the most active metal free catalysts [5,24,33,37,38,42,47–50] for OER (for more comparison see Table S2). It is noteworthy that the performance of 20-NMWNT is comparable to that of the most active metal-free catalysts reported very recently including N,S-CNT [47] ($\eta_{\text{OER}10}$ of 360 mV in 1 M KOH), the most active N-doped metal-free catalyst, N-doped graphene nanoribbons (N-GRW) which has been recently reported by Liu et al. [37], showing $\eta_{\text{OER}10}$ of 360 mV in 1 M KOH, and also nitrogen, phosphorus and oxygen tri-doped porous graphite carbon@oxidized carbon cloth (ONPPGC/OCC) [38] developed as a metal-free bifunctional electrocatalyst but requiring significantly higher $\eta_{\text{OER}10}$ of 410 mV in 1 M KOH. Another recent work based on nitrogen and carbon-containing materials has investigated cobalt embedded in porous N-rich carbon (PNC/Co) [44] that requires $\eta_{\text{OER}10}$ of 370 mV in 1 M KOH. These overpotentials are notably higher than that of 20-NMWNT (320 mV). Fig. 3d shows the Tafel plots of 20-NMWNT in OER derived from Fig. 3c 20-NMWNT resulted in Tafel slopes of 78 and 68 mV/decade in 0.1 and 1 M NaOH, respectively. The Tafel plots with good linearity and small slopes imply that 20-NMWNT is an efficient catalyst for OER with a high electrical conductivity for fast electron transfer. Hence, 20-NMWNT is introduced as a novel metal free catalyst for OER with

an activity that rivals the most active reported electrocatalysts for OER so far (Table S2).

2.2. HER electrocatalytic activity

In addition to the superb OER performance discussed above, HER activity of the NMWNT catalyst is also evaluated in N_2 -saturated 0.1 M NaOH to demonstrate potential application of NMWNT as a bifunctional catalyst for full water splitting. Fig. 4 shows polarization curves of HER on the 20-NMWNT material compared with pristine MWNT and 20 wt% Pt/C electrodes. All the measured catalysts are deposited on a GC electrode with a similar loading of $\sim 0.2 \text{ mg cm}^{-2}$. As shown in Fig. 4 the NMWNT electrocatalyst reveals a significant enhancement in HER activity in comparison to the pristine MWNT, comparable to that of the state-of-the-art Pt/C especially at high currents. For the NMWNT an overpotential of 340 mV is required to achieve 10 mA cm^{-2} ($\eta_{\text{HER}10}$) in 0.1 M NaOH which is comparable to that of transition/noble metal and metal free HER catalysts [13,14]. Recently, Co_3O_4 nanospheres on the surface of nitrogen doped carbon nanotubes [25] have been reported for catalyzing full water splitting with higher $\eta_{\text{HER}10}$ of 380 mV in 0.1 M KOH. It should be noted that the activity of 20-NMWNT has a much higher HER activity in comparison with the very recently reported metal-free electrocatalysis in alkaline solutions (N,S-CNT) [47], suggesting a dramatic improvement in HER activity.

We further investigated fabrication of a freestanding electrode by depositing 20-NMWNT on a nickel foam (NF) substrate without any binder. Fig. S5 demonstrates the OER activity of 20-NMWNT/GC, 20-NMWNT/NF in 0.1 M NaOH. The $\eta_{\text{OER}10}$ for the NMWNT/NF is 330 mV indicating higher OER activity of the NMWNT/NF in comparison to the NMWNT/GC. The incorporation of the NF substrate induces significant change for HER in 0.1 M NaOH (Fig. S6 A). The $\eta_{\text{HER}10}$ for the NMWNT/NF is 235 mV. The outstanding bifunctional performance of NMWNT/NF can be attributed to the combined effect of large electrochemically active surface area, efficient mass and charge transport and high structural stability arising from the 3D porous structure of 20-NMWNT/NF. Above all, the porous structure of NF enable efficient transport of reactants (e.g., OH^-) toward and products (e.g., H_2 for HER and O_2 for

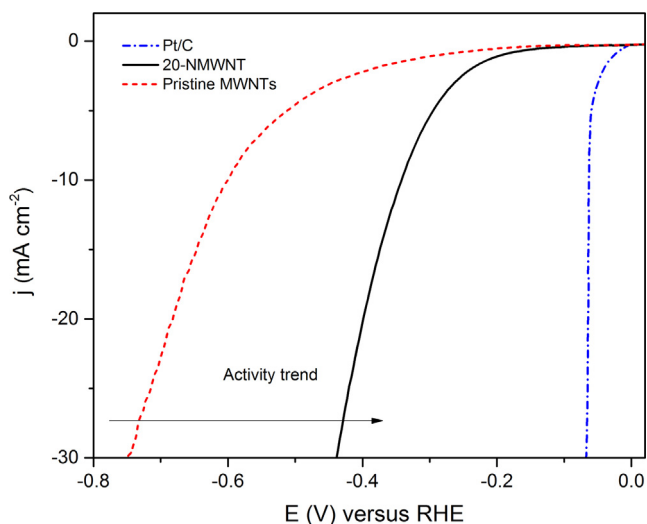


Fig. 4. The HER polarization curves of pristine MWNT (blue dash dotted line), 20-NMWNT (black solid line), and Pt/C (red dashed line). The polarization curves have been reported with iR compensation at a scan rate of 5 mV s^{-1} in 0.1 M NaOH.

OER) away from the catalytic active sites. These remarkable activities for both OER and HER are achieved with a relatively low catalyst loading on the NF ($\sim 0.2 \text{ mg cm}^{-2}$), suggesting very good coupling between the NMWNTs and catalytically active metal based support. This also confirms that the coupling a low amount of the NMWNTs with active metal catalysts can significantly improve the electrocatalytic OER activity.

2.3. Investigating the catalytic active sites of the NMWNT catalyst toward OER and HER

To understand the origin of the activity of the metal free electrocatalysts toward OER and HER, we made an effort to identify the catalytically active OER and HER sites. Pristine MWNT (without any pretreatment) became highly active catalysts with very low amount of nitrogen, demonstrating the crucial role of the nitrogen species. Moreover, high activity of 20-NMWNT for the water electrolysis reported in this work, in comparison to the previously reports on nitrogen doped MWNT [27,51,52], revealed the advantage of the surface doping method used in our study. Through the applied synthesis method, active nitrogen moieties with sufficient interaction with the MWNTs are synthesized. Herein, we try to identify the type of nitrogen moieties which might have the highest activity toward OER/HER and the effect of the interaction between MWNT and ES to enhance the amount of the active sites.

To identify the active N sites for the OER and HER, the 5, 10 and 30-NMWNT samples, synthesized with shorter and longer sonication times, have been also compared with 20-NMWNT. The observed different activities (Fig. S4) suggest differences in nitrogen content and/or moiety type as discussed in the following. Increasing the sonication time from 5 to 20 h resulted in a significant improvement in both OER and HER performances (Fig. S4). Our experiments reveal the 20-NMWNT has the optimal activity for OER/HER since no significant improvement in the activity is observed for longer sonication time (30 h, Fig. S4). To show the influence of the solvent on the activity of the 20-NMWNT, pristine MWNTs was sonicated in the same solution, which was used to synthesize NMWNTs (0.0025 M HCl), for 20 h. As Fig. S5 shows, this sample do not show any significant improvement in the OER

and HER activities compared to those measured for the pristine MWNTs. This shows that the sonication process and the used solution do not solely improve the activity of the MWNTs for HER and OER.

X-ray photoelectron spectroscopy (XPS) is utilized to study the elemental state of the NMWNT catalyst surface and to investigate the nitrogen active sites in the material. Comparison of the N1s XPS spectra of ES, 20, 10 and 5-MWNT/ES is shown in Fig. 5a. Fig. 5b displays N1s region for the 20, 10 and 5-NMWNT catalyst materials. The corresponding elemental compositions from the XPS data are reported in Table S1. The N1s spectra of the ES and the NMWNTs samples have been analyzed by deconvoluting with Gaussian/Lorentzian peaks after removal of a linear background. The N1s spectra of the MWNT/ES is deconvoluted to three main components [53], benzoid amine at $\sim 399.4 \text{ eV}$, oxidized amine at $\sim 401.2 \text{ eV}$, and protonized imine at $\sim 402.6 \text{ eV}$ as shown in Fig. 5. The N1s spectra of the pyrolyzed NMWNT material is deconvoluted to the three main peaks. The first two peaks located at ~ 400.7 and $\sim 398.4 \text{ eV}$ are attributed to the graphitic and pyridinic nitrogen, respectively, while the third peak at $\sim 402.6 \text{ eV}$ corresponds to the protonized imine nitrogen [54–57]. All spectra require an additional wide component around 406 eV representing various oxides and satellite structures. Table 1 shows the concentration of the different nitrogen types in the ES, 5, 10 and 20-MWNT/ES and 5, 10, 20-NMWNT materials.

It is clear from Fig. 5 that the pyrolysis changes the nitrogen bonding in these materials, as the peaks corresponding to graphitic and pyridinic N dominate the spectra after the pyrolysis (Tables S1 and S2). The pyridinic N content is significantly increased from $\sim 0.7 \text{ at.}\%$ in the 5-NMWNT to $\sim 1.3 \text{ at.}\%$ in the 20-NMWNT. It has been reported in the literature that graphitic N serves as the active site for other catalytic reactions, such as oxygen reduction reaction [54,56] while pyridinic N is active toward OER [33,37]. Depending on the N dopant configurations, electron transfer mechanism in N-doped carbon nanomaterials can be either p- or n-type [58,59] as has been shown both theoretically and experimentally [33,37,56,60]. Pyridinic N can accept electrons (p-type doping) from adjacent C atoms, facilitating the adsorption of water oxidation intermediates (OH^- , OOH^-) as the rate-determining steps for

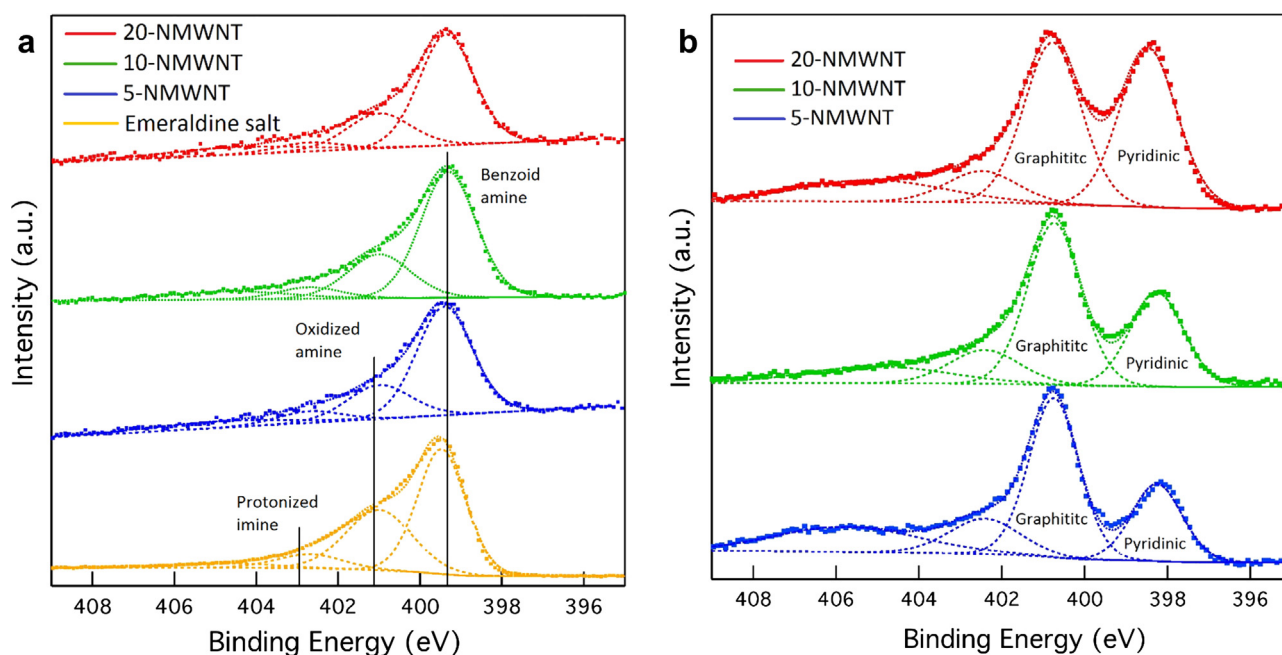


Fig. 5. High-resolution N 1s XPS spectra for the 20-NMWNT, 10-NMWNT and 5-NMWNT materials (a) before pyrolysis and (b) after pyrolysis and at $800 \text{ }^\circ\text{C}$.

Table 1
The relative ratio of pyridinic, benzoid amine, graphitic, oxidized amine, and protonized imine nitrogen to the whole nitrogen content for the emeraldine salt, 5-MWNT/ES, 20-MWNT/ES, 5-NMWNT, 10-NMWNT and 20-NMWNT materials.

Catalyst	Pyridinic nitrogen =N- ~398.4 eV	Benzoid amine or -NH- ~399.4 eV	Graphitic nitrogen ~400.7 eV	Oxidized amine N+ ~401.2 eV	Protonized imine N+ ~402.6 eV
Emeraldine salt	–	55%	–	37%	8%
5-MWNT/ES	–	60%	–	33%	7%
20-MWNT/ES	–	68%	–	25%	7%
5-NMWNT	27%	–	55%	–	18%
10-NMWNT	31%	–	54%	–	15%
20-NMWNT	45%	–	45%	–	10%

OER in alkaline solution [37]. On the other hand, n-type doping has been found for quaternary/pyrrolic N. As a result, the pyridinic nitrogen sites in the NMWNTs catalyst are the active sites for OER and HER, consistent with the recent studies about N active sites for OER [33,37].

The XPS results (Table S1) reveal that the nitrogen content before pyrolysis is decreased from 1.2% in the 5-MWNT/ES sample to 0.5% for the 20-MWNT/ES material. This shows that the amount of ES on MWNT is decrease with the increasing sonication time so that only the ES with a strong interaction with MWNT remains on the nanotube surface. This is in agreement with the thermogravimetric analysis (TGA, Fig. S8) indicating that the amount of the ES in the material is decreased from 28 wt% for the 5-MWNT/ES to 20 wt% for the 20-MWNT/ES. However, XPS data show that after the pyrolysis the N content is almost the same for all the samples (Table S1).

It is noteworthy, that 5-MWNT/ES, with clearly higher amount of ES in comparison to the 20-MWNT/ES material, results in a catalyst with lower activities for HER and OER, after the pyrolysis (Fig. S4). Reason for this is that the longer sonication time opens MWNTs bundles after which the polymer salt has a better access to the surface of the MWNTs. Hence, for 20-MWNT/ES this treatment induces intimate contact between ES and MWNT, leading to a better integration of the nitrogen moieties into the surface of the MWNT. This provides more active nitrogen sites toward both OER and HER at the high carbonization temperature (800 °C) as discussed above in the context of XPS measurements (Table 1). More specifically, graphitization at high temperature acts as a switch for transferring inactive nitrogen sites, properly attached on the MWNT surface, to the active sites [25]. These results reveal an important finding for nitrogen functionalized carbon nanotubes: Since the pyrolyzed polymer interacts with CNTs through π - π^* interaction it is plausible that the nitrogen moieties formed during the pyrolysis are not incorporated in the CNT lattice. Hence, the catalytic activity of these materials depends more on the interaction of nitrogen moieties with the nanotubes rather than the amount of nitrogen containing compound provided on the tubes. In general, three important parameters affecting catalytic activity of such a catalyst material should be taken into consideration: (i) the structure of the catalyst support (MWNTs), (ii) the structure of the functionalities (pyrolyzed ES) providing the active sites, and (iii) the interaction between the functionalities and the support. So interaction of electronic states of the CNT support and the pyrolyzed ES takes place affecting the catalytic behavior of the N functionalities on the sidewall of the MWNTs. The effect of the MWNT structure in this interaction and activity is complicated as a number of parameters, such as MWNT diameter and chirality, determine its electronic density of states [61–63]. It is also noteworthy that the polymer wrapping in this synthesis method is applied for the pristine MWNT, instead of the mostly used acid treated tubes, and thus the oxygen content in the NMWNTs (Table S1) is much lower than that reported for other N-doped materials [33]. This is important for the stability of the electrocat-

alysts. Furthermore, in the MWNTs, no metal impurity is detected by XPS (Table S1), in agreement with the TEM images (Fig. 2 and Fig. S1), further suggesting that the activity of the NMWNT materials comes from the nitrogen active sites.

To evaluate the intrinsic activity of the catalyst the turnover frequency (TOF, defined as the number of O₂ molecules evolved per second per active site) is employed (see the Supplementary Information for details). The corresponding TOF is ~ 0.07 s⁻¹ for the NMWNT catalyst, calculated at overpotential of 320 mV in 1 M NaOH by assuming that the pyridinic nitrogen as active sites for OER and mechanisms obeys the four-electron transfer pathway [33,37]. However, the reported TOF is an approximate value since the exact amount of N on the surface is higher than 1.3 at.% as MWNT consists of several coaxial carbo nanotube layers but nitrogen is only located on the surface. Hence, the surface N to C ratio can be higher than obtained from the XPS measurements.

Fig. 6 shows Raman spectra of 20-NMWNT and pristine MWNT. The band at ~ 1330 cm⁻¹ (D-band) originates from atomic displacement and disorder induced features caused by lattice defects in graphitic structure of MWNT. The band at ~ 1590 cm⁻¹ (G-band) indicates the formation of well-graphitized carbon nanotubes [64] and represents the tangential vibration of carbon atoms in graphene sheets [65]. The G-band of the 20-NMWNT sample undergoes a down-shift with respect to that of MWNT from 1603 to 1598 cm⁻¹ (Fig. 6). This shift of the G-band can be ascribed to C–C expansion (or contraction) and the changes of electronic structure [64]. The change in the electronic structure of NMWNT, relative to the MWNT, may be associated directly to the amount and type of incorporated nitrogen [66]. The nitrogen atoms can

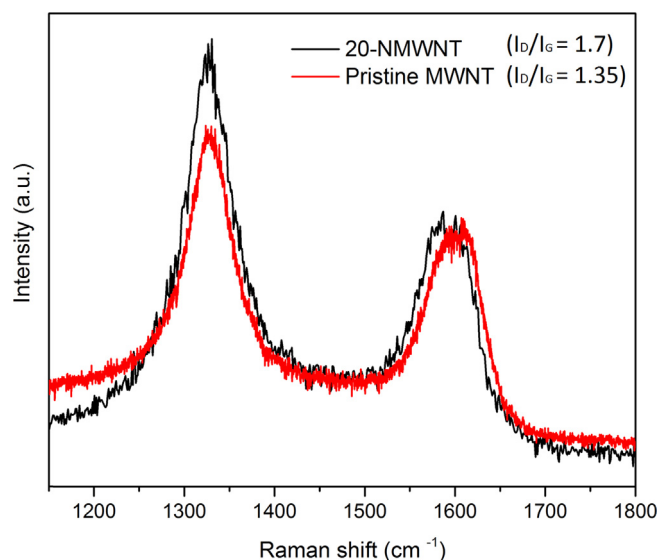


Fig. 6. Raman spectra for pristine MWNT (red line) and 20-NMWNT (black line).

act as either electron donor or acceptor when CNTs are doped with nitrogen [56]. Here, the down-shift of the G-band may imply an enhanced electron transfer between valance and conduction bands, which is in accordance with the earlier reported results [64,67]. The intensity ratio of the D and G band (I_D/I_G) indicates the degree of disorder in carbon materials and slightly increases from 1.35 for the pristine MWNT to 1.7 for 20-NMWNT. This change is attributed to incorporation of N atoms in the carbon lattice of MWNT. Carroll et al. [68], reported that for N doped CNTs, the D-band intensity is more sensitive to pyridinic defects than to graphitic ones. It is consistent with the Raman spectra in Fig. S9 showing that the I_D/I_G ratio of 5 and 10-NMWNT (1.4 and 1.43, respectively) is smaller than that of 20-NMWNT.

2.4. Stability

In energy conversion systems, one vital challenge for efficient HER and OER catalysts, or the catalyst supports, is the long-term stability during electrolysis. The stability issue for OER is even more pronounced as materials have to survive in the strongly oxidative environment of electrolyzers that can induce changes on the structure of the catalyst [3]. For stability measurement of NMWNT, nickel foam has been utilized as the electrode substrate (NMWNT/NF) since the adhesion of NMWNT on the NF is better than on the GC. Fig. 7 shows measured time dependencies of the current density at a static potential of 1.56 and -0.23 V for OER and HER, respectively. These potentials correspond the current density of ~ 10 mA cm^{-2} for both OER and HER. The chronoamperometric curves in 0.1 M NaOH show that the current densities remain stable for OER and HER during 24 h of the continuous half-cell reaction. The OER stability is also investigated in 0.1 M NaOH by cycling the potential between 1 and 1.7 V at a scan rate of 50 mV s^{-1} (Fig. S10). No significant degradation is observed in the OER polarization curve for the 20-NMWNT/NF after 1000 potential cycles.

These stability results are also remarkable compared to the other published studies for the metal-free electrocatalysts, for both OER and HER [33,49]. These results indicate that our facile synthesis method provides high interaction between the ES and MWNT, resulting in a better integration of nitrogen into the surface of the nanotubes, and consequently leading to exceptionally active N-doped CNTs with excellent stability in alkaline media.

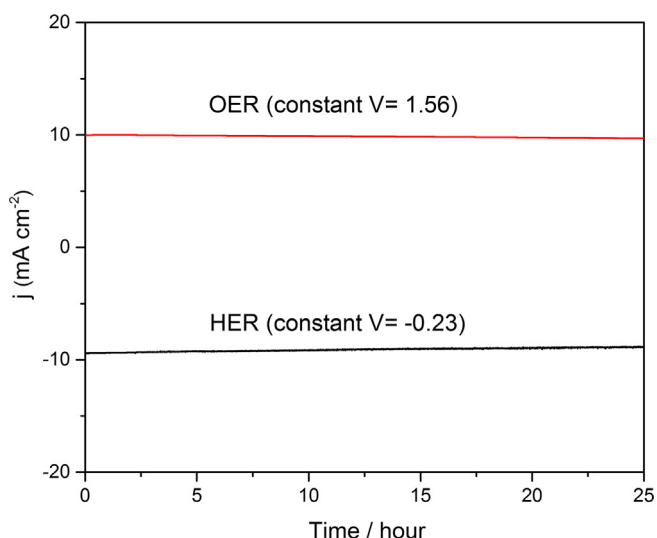


Fig. 7. Chronoamperometric curves of OER and HER on 20-NMWNT/NF at constant potentials of 1.56 V and -0.23 V, respectively, in 0.1 M NaOH.

It is noteworthy that this excellent stability of 20-NMWNT for both OER and HER is more confirmed with XPS analysis. Tables S3 and S4 show the relative amounts of different types of nitrogen and elemental composition of 20-NMWNT before and after electrochemical measurements, respectively. The observed changes in the pyridinic (43–45%) and quaternary nitrogen contents (45–48%) relative to the whole N content are within the experimental error. After the electrochemical measurements, as it is expected at the high OER potential range, oxygen concentration on the surface increases whereas N/C ratio is practically unchanged. These results show the potential of 20-NMWNT as an ultra-high active and stable metal-free bifunctional electrocatalysts for full water-splitting in alkaline media.

3. Conclusion

In conclusion, we have developed a facile and scalable post-treatment method for synthesizing bifunctional nitrogen functionalized carbon nanotubes (NMWNTs) allowing control of the type of formed nitrogen moieties. In this method, a polymer salt containing positively charged nitrogen moieties enhances the interaction with MWNTs via the intermolecular charge-transfer. In this method, the polymer is efficiently wrapped around the pristine MWNTs and then graphitized at a high temperature to form NMWNTs. The resulting material functions as an electrocatalyst with high activity and durability toward both OER and HER in alkaline media. As far as we are aware, resultant 20-NMWNT exhibits the best OER catalytic activity as a metal-free electrocatalyst and its activity is even comparable to that of the state-of-the-art metal-based catalysts. 20-NMWNT also is one of the most active HER metal-free catalysts comparable to the highly active Pt/C at high overpotentials. The OER activity of the 20-NMWNT catalyst reveals significant improvement in comparison to other metal-free electrocatalysts for OER so that its activity is even comparable to that of the state-of-the-art metal-based catalysts. It is shown that the interaction of the polymer salt with the MWNT plays an important role in the formation of the final type of the nitrogen functionalities and HER/OER activities. It is revealed that pyridinic N serves as the highest active site, compared to other nitrogen types, toward both OER and HER. The NMWNT catalyst shows also excellent stability for the long-term continuous water electrolysis. The HER/OER activity of the NMWNTs is further improved by the coupling the catalysts on nickel foam to form a 3D flexible porous electrode for HER/OER. This shows the potential of the NMWNTs for coupling with other active metal catalysts in the future.

Furthermore, because of the high conductivity and large surface area, the NMWNTs can also function as novel catalyst supports inducing potentially synergistic effect for decorating active metal nanoparticles. As far as we are aware, these are the first experimental evidences indicating a facile method to change the ratio of the different types of N species in the N functionalized carbon nanomaterials to improve the catalytic activity toward full water splitting. These results are important for further rational improvement of this already highly active bifunctional metal-free electrocatalyst material.

Acknowledgments

This work is supported by Academy of Finland (the DEMEC, CloseLoop and CIRCLE projects), Aalto University (the MOPPI project in AEF program) and EU Horizon 2020 (the CREATE project). This work made use of the Aalto University Nanomicroscopy Center (Aalto-NMC) premises and the RaMI Raw Material infrastructure.

Appendix A. Supplementary material

Supplementary data associated with this article can be found, in the online version, at <http://dx.doi.org/10.1016/j.jcat.2017.07.001>.

References

- [1] Y. Jiao, Y. Zheng, M. Jaroniec, S.Z. Qiao, Design of electrocatalysts for oxygen- and hydrogen-involving energy conversion reactions, *Chem. Soc. Rev.* 44 (2015) 2060–2086, <http://dx.doi.org/10.1039/C4CS00470A>.
- [2] J. Duan, S. Chen, M. Jaroniec, S.Z. Qiao, Heteroatom-doped graphene-based materials for energy-relevant electrocatalytic processes, *ACS Catal.* 5 (2015) 5207–5234, <http://dx.doi.org/10.1021/acscatal.5b00991>.
- [3] M. Tavakkoli, T. Kallio, O. Reynaud, A.G. Nasibulin, J. Sainio, H. Jiang, E.I. Kauppinen, K. Laasonen, Maghemite nanoparticles decorated on carbon nanotubes as efficient electrocatalysts for the oxygen evolution reaction †, *J. Mater. Chem. A Mater. Energy Sustain.* 4 (2016) 5216–5222, <http://dx.doi.org/10.1039/C6TA01472K>.
- [4] I.H. Kwak, H.S. Im, D.M. Jang, Y.W. Kim, K. Park, Y.R. Lim, E.H. Cha, J. Park, CoSe₂ and NiSe₂ nanocrystals as superior bifunctional catalysts for electrochemical and photoelectrochemical water splitting, *ACS Appl. Mater. Interfaces.* 8 (2016) 5327–5334, <http://dx.doi.org/10.1021/acsami.5b12093>.
- [5] A.M. El-Sawy, I.M. Mosa, D. Su, C.J. Guild, S. Khalid, R. Joesten, J.F. Rusling, S.L. Suib, Controlling the active sites of sulfur-doped carbon nanotube-graphene nanobelts for highly efficient oxygen evolution and reduction catalysis, *Adv. Energy Mater.* 6 (2016) 1–12, <http://dx.doi.org/10.1002/aenm.201501966>.
- [6] W. Zhu, X. Yue, W. Zhang, S. Yu, Y. Zhang, J. Wang, J. Wang, Nickel sulfide microsphere film on Ni foam as an efficient bifunctional electrocatalyst for overall water splitting, *Chem. Commun.* 52 (2016) 1486–1489, <http://dx.doi.org/10.1039/c5cc08064a>.
- [7] B. You, N. Jiang, M. Sheng, M.W. Bhushan, Y. Sun, Hierarchically porous urchin-like Ni₂P superstructures supported on nickel foam as efficient bifunctional electrocatalysts for overall water splitting, *ACS Catal.* 6 (2016) 714–721, <http://dx.doi.org/10.1021/acscatal.5b02193>.
- [8] C. Xiao, Y. Li, X. Lu, C. Zhao, Bifunctional Porous NiFe/NiCo₂O₄/Ni foam electrodes with triple hierarchy and double synergies for efficient whole cell water splitting, *Adv. Funct. Mater.* (2016) 3515–3523, <http://dx.doi.org/10.1002/adfm.201505302>.
- [9] Y. Feng, H. Zhang, L. Fang, Y. Mu, Y. Wang, Uniquely Monodispersing NiFe Alloyed Nanoparticles in Three-Dimensional Strongly Linked Sandwiched Graphitized Carbon Sheets for High-Efficiency Oxygen Evolution Reaction (2016), <http://dx.doi.org/10.1021/acscatal.6b00481>.
- [10] C.C.L. McCrory, S. Jung, J.C. Peters, T.F. Jaramillo, Benchmarking heterogeneous electrocatalysts for the oxygen evolution reaction, *J. Am. Chem. Soc.* 135 (2013) 16977–16987, <http://dx.doi.org/10.1021/ja407115p>.
- [11] C.C.L. McCrory, S. Jung, I.M. Ferrer, S.M. Chatman, J.C. Peters, T.F. Jaramillo, Benchmarking hydrogen evolving reaction and oxygen evolving reaction electrocatalysts for solar water splitting devices, *J. Am. Chem. Soc.* 137 (2015) 4347–4357, <http://dx.doi.org/10.1021/ja510442p>.
- [12] Y. Xu, M. Kraft, R. Xu, Metal-free carbonaceous electrocatalysts and photocatalysts for water splitting, *Chem. Soc. Rev.* 45 (2016) 3039–3052, <http://dx.doi.org/10.1039/c5cs00729a>.
- [13] N. Danilovic, R. Subbaraman, D. Strmcnik, K.C. Chang, A. P. Paulikas, V.R. Stamenkovic, N.M. Markovic, Enhancing the alkaline hydrogen evolution reaction activity through the bifunctionality of Ni(OH)₂/metal catalysts, *Angew. Chemie – Int. Ed.* 51 (2012) 12495–12498, doi:10.1002/anie.201204842.
- [14] H. Jiang, Y. Zhu, Y. Su, Y. Yao, Y. Liu, X. Yang, C. Li, Highly dual-doped multilayer nanoporous graphene: efficient metal-free electrocatalysts for the hydrogen evolution reaction, *J. Mater. Chem. A* 3 (2015) 12642–12645, <http://dx.doi.org/10.1039/C5TA02792F>.
- [15] Y. Yang, H. Fei, G. Ruan, L. Li, G. Wang, N.D. Kim, J.M. Tour, Carbon-free electrocatalyst for oxygen reduction and oxygen evolution reactions, *ACS Appl. Mater. Interfaces* 7 (2015) 20607–20611, <http://dx.doi.org/10.1021/acsami.5b04887>.
- [16] J. Wang, H.X. Zhong, Z.L. Wang, F.L. Meng, X.B. Zhang, Integrated three-dimensional carbon paper/carbon tubes/cobalt-sulfide sheets as an efficient electrode for overall water splitting, *ACS Nano* 10 (2016) 2342–2348, <http://dx.doi.org/10.1021/acsnano.5b07126>.
- [17] N. Jiang, B. You, M. Sheng, Y. Sun, Bifunctionality and mechanism of electrodeposited nickel-phosphorous films for efficient overall water splitting, *ChemCatChem* 8 (2016) 106–112, <http://dx.doi.org/10.1002/cctc.201501150>.
- [18] T. Liu, A.M. Asiri, X. Sun, Electrodeposited Co-doped NiSe₂ nanoparticles film: a good electrocatalyst for efficient water splitting, *Nanoscale* 8 (2016) 3911–3915, <http://dx.doi.org/10.1039/c5nr07170d>.
- [19] L. Stern, L. Feng, F. Song, X. Hu, Ni₂P as a Janus catalyst for water splitting: the oxygen evolution activity of Ni₂P nanoparticles, *Energy Environ. Sci.* 8 (2015) 23417–23251, <http://dx.doi.org/10.1039/C5EE01155H>.
- [20] J. Luo, J. Im, M.T. Mayer, M. Schreier, M.K. Nazeeruddin, N. Park, S.D. Tilley, H.J. Fan, M. Grätzel, Water photolysis at 12.3% efficiency via perovskite photovoltaics and Earth-abundant catalysts, 2014.
- [21] V. Artero, M. Chavarot-kerlidou, M. Fontecave, Splitting water with cobalt, *Angew. Chem.* 50 (2011) 7238–7266, <http://dx.doi.org/10.1002/anie.201007987>.
- [22] R. Li, Z. Wei, X. Gou, Nitrogen and phosphorus dual-doped graphene/carbon nanosheets as bifunctional electrocatalysts for oxygen reduction and evolution, *ACS Catal.* 5 (2015) 4133–4142, <http://dx.doi.org/10.1021/acscatal.5b00601>.
- [23] S. Gadipelli, T. Zhao, S.A. Shevlin, Z. Guo, Environmental science switching effective oxygen reduction and graphitization of a cobalt – nitrogen – carbon framework system †, *Energy Environ. Sci.* 9 (2016) 1661–1667, <http://dx.doi.org/10.1039/C6EE00551A>.
- [24] S. Chen, J. Duan, M. Jaroniec, S.Z. Qiao, Nitrogen and oxygen dual-doped carbon hydrogel film as a substrate-free electrode for highly efficient oxygen evolution reaction, *Adv. Mater.* 26 (2014) 2925–2930, <http://dx.doi.org/10.1002/adma.201305608>.
- [25] T. Sharifi, E. Gracia-Espino, X. Jia, R. Sandström, T. Wågberg, Comprehensive study of an earth-abundant bifunctional 3D electrode for efficient water electrolysis in alkaline medium, *ACS Appl. Mater. Interfaces* 7 (2015) 28148–28155, <http://dx.doi.org/10.1021/acsami.5b10118>.
- [26] W. Xi, Z. Ren, L. Kong, J. Wu, S. Du, J. Zhu, Y. Xue, H. Meng, H. Fu, Dual-valence nickel nanosheets covered with thin carbon as bifunctional electrocatalysts for full water splitting †, *J. Mater. Chem. A Mater. Energy Sustain.* (2016) 1–8, <http://dx.doi.org/10.1039/C6TA00894A>.
- [27] Y. Zheng, Y. Jiao, Y. Zhu, L.H. Li, Y. Han, Y. Chen, A. Du, M. Jaroniec, S.Z. Qiao, Hydrogen evolution by a metal-free electrocatalyst., *Nat. Commun.* 5 (2014) 3783, doi:10.1038/ncomms4783.
- [28] Y. Zheng, Y. Jiao, L. Ge, M. Jaroniec, S.Z. Qiao, Two-step boron and nitrogen doping in graphene for enhanced synergistic catalysis, *Angew. Chemie – Int. Ed.* 52 (2013) 3110–3116, <http://dx.doi.org/10.1002/anie.201209548>.
- [29] W. Cui, Q. Liu, N. Cheng, A.M. Asiri, X. Sun, Activated carbon nanotubes: a highly-active metal-free electrocatalyst for hydrogen evolution reaction, *Chem. Commun. (Camb.)* 50 (2014) 9340–9342, <http://dx.doi.org/10.1039/c4cc02713b>.
- [30] J. Zhang, Z. Zhao, Z. Xia, L. Dai, A metal-free bifunctional electrocatalyst for oxygen reduction and oxygen evolution reactions, *Nat. Nanotechnol.* 10 (2015) 444–452, <http://dx.doi.org/10.1038/nnano.2015.48>.
- [31] Z.L. Wang, X.F. Hao, Z. Jiang, X.P. Sun, D. Xu, J. Wang, H.X. Zhong, F.L. Meng, X.B. Zhang, C and N hybrid coordination derived Co-C-N complex as a highly efficient electrocatalyst for hydrogen evolution reaction, *J. Am. Chem. Soc.* 137 (2015) 15070–15073, <http://dx.doi.org/10.1021/jacs.5b09021>.
- [32] K. Qu, Y. Zheng, S. Dai, S.Z. Qiao, Graphene oxide-polydopamine derived N, S-codoped carbon nanosheets as superior bifunctional electrocatalysts for oxygen reduction and evolution, *Nano Energy* 19 (2016) 373–381, <http://dx.doi.org/10.1016/j.nanoen.2015.11.027>.
- [33] Y. Zhao, R. Nakamura, K. Kamiya, S. Nakanishi, K. Hashimoto, Nitrogen-doped carbon nanomaterials as non-metal electrocatalysts for water oxidation, *Nat. Commun.* 4 (2013) 1–7, <http://dx.doi.org/10.1038/ncomms3390>.
- [34] T. Fujigaya, J. Morita, N. Nakashima, Grooves of bundled single-walled carbon nanotubes dramatically enhance the activity of the oxygen reduction reaction, *ChemCatChem* 6 (2014) 3169–3173, <http://dx.doi.org/10.1002/cctc.201402565>.
- [35] T. Fujigaya, T. Uchinoumi, K. Kaneko, N. Nakashima, Design and synthesis of nitrogen-containing calcined polymer/carbon nanotube hybrids that act as a platinum-free oxygen reduction fuel cell catalyst, *Chem. Commun.* 47 (2011) 6843, <http://dx.doi.org/10.1039/c1cc11303h>.
- [36] J. Yang, T. Fujigaya, N. Nakashima, Decorating unoxidized-carbon nanotubes with homogeneous Ni-Co spinel nanocrystals show superior performance for oxygen evolution/reduction reactions, *Sci. Rep.* 7 (2017) 45384, <http://dx.doi.org/10.1038/srep45384>.
- [37] H. Bin Yang, J. Miao, S.-F. Hung, J. Chen, H.B. Tao, X. Wang, L. Zhang, R. Chen, J. Gao, H.M. Chen, L. Dai, B. Liu, Identification of catalytic sites for oxygen reduction and oxygen evolution in N-doped graphene materials: development of highly efficient metal-free bifunctional electrocatalyst, *Sci. Adv.* 2 (2016), <http://dx.doi.org/10.1126/sciadv.1501122>, 1501122.
- [38] J. Lai, S. Li, F. Wu, M. Saqib, R. Luque, G. Xu, Unprecedented metal-free 3D porous carbonaceous electrodes for full water splitting, *Energy Environ. Sci.* 9 (2016) 1210–1214, <http://dx.doi.org/10.1039/C5EE02996A>.
- [39] X. Yan, Z. Han, Y. Yang, B. Tay, Fabrication of carbon nanotube – polyaniline composites via electrostatic adsorption in aqueous colloids fabrication of carbon nanotube – polyaniline composites via electrostatic adsorption in aqueous colloids, *J. Phys. Chem. C* 3 (2007) 4125–4131, <http://dx.doi.org/10.1021/jp0651844>.
- [40] S. Wang, D. Yu, L. Dai, Polyelectrolyte functionalized carbon nanotubes as efficient, *J. Am. Chem. Soc.* 133 (2011) 5182–5185.
- [41] M. Tavakkoli, T. Kallio, O. Reynaud, A.G. Nasibulin, J. Sainio, H. Jiang, E.I. Kauppinen, K. Laasonen, Maghemite nanoparticles decorated on carbon nanotubes as efficient electrocatalysts for the oxygen evolution reaction., *J. Mater. Chem. A Mater. Energy Sustain.* 4 (2016) 5216–5222, doi:10.1039/C6TA01472K.
- [42] T.Y. Ma, S. Dai, M. Jaroniec, S.Z. Qiao, Graphitic carbon nitride nanosheet-carbon nanotube three-dimensional porous composites as high-performance oxygen evolution electrocatalysts, *Angew. Chemie – Int. Ed.* 53 (2014) 7281–7285, <http://dx.doi.org/10.1002/anie.201403946>.
- [43] J. Suntivich, K.J. May, H.A. Gasteiger, J.B. Goodenough, Y. Shao-Horn, A Perovskite oxide optimized for oxygen evolution catalysis from molecular

- orbital principles, *Science* (80) 334 (2011) 1383–1385. doi:10.1126/science.1212858.
- [44] X. Li, Z. Niu, J. Jiang, L. Ai, Cobalt nanoparticles embedded in porous N-rich carbon as an efficient bifunctional electrocatalyst for water splitting †, *J. Mater. Chem. A Mater. Energy Sustain.* 4 (2016) 3204–3209, <http://dx.doi.org/10.1039/C6TA000223D>.
- [45] X. Zhang, H. Xu, X. Li, Y. Li, T. Yang, Y. Liang, Facile synthesis of nickel-iron/nanocarbon hybrids as advanced electrocatalysts for efficient water splitting, *ACS Catal.* 6 (2016) 580–588, <http://dx.doi.org/10.1021/acscatal.5b02291>.
- [46] Y.P. Zhu, Y.P. Liu, T.Z. Ren, Z.Y. Yuan, Self-supported cobalt phosphide mesoporous nanorod arrays: a flexible and bifunctional electrode for highly active electrocatalytic water reduction and oxidation, *Adv. Funct. Mater.* (2015) 7337–7347, <http://dx.doi.org/10.1002/adfm.201503666>.
- [47] K. Qu, Y. Zheng, Y. Jiao, X. Zhang, S. Dai, S.-Z. Qiao, Polydopamine-inspired, dual heteroatom-doped carbon nanotubes for highly efficient overall water splitting, *Adv. Energy Mater.* (2016) 1602068. doi:10.1002/aenm.201602068.
- [48] J. Liu, S. Zhao, C. Li, M. Yang, Y. Yang, Y. Liu, Y. Lifshitz, S.T. Lee, Z. Kang, Carbon nanodot surface modifications initiate highly efficient, stable catalysts for both oxygen evolution and reduction reactions, *Adv. Energy Mater.* 6 (2016), <http://dx.doi.org/10.1002/aenm.201502039>.
- [49] X. Lu, W.L. Yim, B.H.R. Suryanto, C. Zhao, Electrocatalytic oxygen evolution at surface-oxidized multiwall carbon nanotubes, *J. Am. Chem. Soc.* 137 (2015) 2901–2907, <http://dx.doi.org/10.1021/ja509879r>.
- [50] T.Y. Ma, J. Ran, S. Dai, M. Jaroniec, S.Z. Qiao, Phosphorus-doped graphitic carbon nitrides grown in situ on carbon-fiber paper: flexible and reversible oxygen electrodes, *Angew. Chemie – Int. Ed.* 54 (2015) 4646–4650, <http://dx.doi.org/10.1002/anie.201411125>.
- [51] G.L. Tian, Q. Zhang, B. Zhang, Y.G. Jin, J.Q. Huang, D.S. Su, F. Wei, Toward full exposure of “active Sites”: nanocarbon electrocatalyst with surface enriched nitrogen for superior oxygen reduction and evolution reactivity, *Adv. Funct. Mater.* 24 (2014) 5956–5961, <http://dx.doi.org/10.1002/adfm.201401264>.
- [52] Y. Yao, B. Zhang, J. Shi, Q. Yang, Preparation of nitrogen-doped carbon nanotubes with different morphologies from melamine-formaldehyde resin, *ACS Appl. Mater. Interfaces.* 7 (2015) 7413–7420, <http://dx.doi.org/10.1021/acsami.5b01233>.
- [53] S. Golczak, A. Kancierzewska, M. Fahlman, K. Langer, J.J. Langer, Comparative XPS surface study of polyaniline thin films, *Solid State Ionics* 179 (2008) 2234–2239, <http://dx.doi.org/10.1016/j.ssi.2008.08.004>.
- [54] P. Chen, T.Y. Xiao, Y.H. Qian, S.S. Li, S.H. Yu, A nitrogen-doped graphene/carbon nanotube nanocomposite with synergistically enhanced electrochemical activity, *Adv. Mater.* 25 (2013) 3192–3196, <http://dx.doi.org/10.1002/adma.201300515>.
- [55] T. Sharifi, F. Nitze, H.R. Barzegar, C.W. Tai, M. Mazurkiewicz, A. Malolepszy, L. Stobinski, T. Wågberg, Nitrogen doped multi walled carbon nanotubes produced by CVD-correlating XPS and Raman spectroscopy for the study of nitrogen inclusion, *Carbon N. Y.* 50 (2012) 3535–3541, <http://dx.doi.org/10.1016/j.carbon.2012.03.022>.
- [56] T. Sharifi, G. Hu, X. Jia, T. Wågberg, Formation of active sites for oxygen reduction reactions by transformation of nitrogen functionalities in nitrogen-doped carbon nanotubes, *ACS Nano* 6 (2012) 8904–8912, <http://dx.doi.org/10.1021/nn302906r>.
- [57] J.R. Pels, F. Kapteijn, J.A. Moulijn, Q. Zhu, K.M. Thomas, Evolution of nitrogen functionalities in carbonaceous materials during pyrolysis, *Carbon N. Y.* 33 (1995) 1641–1653, [http://dx.doi.org/10.1016/0008-6223\(95\)00154-6](http://dx.doi.org/10.1016/0008-6223(95)00154-6).
- [58] W.J. Lee, U.N. Maiti, J.M. Lee, J. Lim, T.H. Han, S.O. Kim, Nitrogen-doped carbon nanotubes and graphene composite structures for energy and catalytic applications, *Chem. Commun.* 50 (2014) 6818–6830, <http://dx.doi.org/10.1039/c4cc00146j>.
- [59] B.F.R. Czerw*, † M. Terrones, ‡ § J.-C. Charlier, | X. Blase, W.B. R. Kamalakara, † N. Grobert, ¶ H. Terrones, § D. Tekleab, † P.M. Ajayan, D.L.C.M. Ru2hle, Identification of electron donor states in N-doped carbon nanotubes, *Nano Lett.* 1 (2001) 457–460. doi: 10.1021/nl015549q.
- [60] W. Ding, Z. Wei, S. Chen, X. Qi, T. Yang, J. Hu, D. Wang, L. Wan, S.F. Alvi, L. Li, Space-confinement-induced synthesis of pyridinic-and pyrrolic-nitrogen-doped graphene for the catalysis of oxygen reduction, *Angew. Chemie.* 125 (2013) 11971–11975, <http://dx.doi.org/10.1002/anie.201303924>.
- [61] J.M. Planeix, N. Coustel, B. Coq, V. Brotons, P.S. Kumbhar, R. Dutartre, P. Geneste, P. Bernier, P.M. Ajayan, Application of carbon nanotubes as supports in heterogeneous catalysis, *J. Power Sources* 116 (1994) 7935–7936, <http://dx.doi.org/10.1021/ja00096a076>.
- [62] H. Ma, L. Wang, L. Chen, C. Dong, W. Yu, T. Huang, Y. Qian, Pt nanoparticles deposited over carbon nanotubes for selective hydrogenation of cinnamaldehyde, *Catal. Commun.* 8 (2007) 452–456, <http://dx.doi.org/10.1016/j.catcom.2006.07.020>.
- [63] T. Bligaard, Linear energy relations and the computational design of selective hydrogenation/dehydrogenation catalysts, *Angew. Chemie Int. Ed.* 48 (2009) 9782–9784, <http://dx.doi.org/10.1002/anie.200905141>.
- [64] H. Liu, Y. Zhang, R. Li, X. Sun, S. Désilets, H. Abou-Rachid, M. Jaidann, L.S. Lussier, Structural and morphological control of aligned nitrogen-doped carbon nanotubes, *Carbon N. Y.* 48 (2010) 1498–1507, <http://dx.doi.org/10.1016/j.carbon.2009.12.045>.
- [65] M.S. Dresselhaus, G. Dresselhaus, R. Saito, A. Jorio, Raman spectroscopy of carbon nanotubes, *Phys. Rep.* 409 (2005) 47–99, <http://dx.doi.org/10.1016/j.physrep.2004.10.006>.
- [66] J.F. Cardenas, Protonation and sonication effects on aggregation sensitive Raman features of single wall carbon nanotubes, *Carbon N. Y.* 46 (2008) 1327–1330, <http://dx.doi.org/10.1016/j.carbon.2008.05.015>.
- [67] Z. Chen, D. Higgins, H. Tao, R.S. Hsu, Z. Chen, Highly active nitrogen-doped carbon nanotubes for oxygen reduction reaction in fuel cell applications, *J. Phys. Chem. C* 113 (2009) 21008–21013, <http://dx.doi.org/10.1021/jp908067v>.
- [68] J. Liu, S. Webster, D.L. Carroll, Temperature and flow rate of NH₃ effects on nitrogen content and doping environments of carbon nanotubes grown by injection CVD method, *J. Phys. Chem. B* 109 (2005) 15769–15774, <http://dx.doi.org/10.1021/jp050123b>.